Proceedings of the 21st ICSMGE, Vienna, Austria, 14 – 19 June 2026. Pistrol, Adam & Schweiger (eds.)
Published by: ÖGG, Austrian Society for Geomechanics, Salzburg, Austria, ISBN 978-3-9503898-4-5
https://doi.org/10.53243/ICSMGE2026-1571

Crack propagation mechanisms in dams and levees caused by vertical offsets in the foundation

Kil-Wan Ko
Civil and Environmental Engineering, Korea Advanced Institute of Science and Technology, Daejeon, Republic of Korea

Mark J. Bancroft, Jason DeJong, Dan Wilson, Ross W. Boulanger
Civil and Environmental Engineering, University of California, Davis, CA, USA, jdejong@ucdavis.edu

Jack Montgomery
Civil and Environmental Engineering, Auburn University, Auburn, AL, USA

Grace Chen, Steven Friesen
California Department of Water Resources, Sacramento, CA, USA

ABSTRACT: Levees and dams constructed across active faults face a risk of failure due to the formation of transverse cracks induced by a vertical offset in the foundation and the subsequent initiation and progression of concentrated leak erosion (CLE). The present understanding of crack formation, developed from a limited set of case histories and numerical simulations, includes large uncertainties, and the empirical methods used to estimate crack potential and extent are based on simplified geometries and limited data. A research program was undertaken to better understand mechanisms of crack formation and propagation using the 9m radius centrifuge at the University of California at Davis. A model test was performed at 40g to simulate a levee/dam with a height of 10 m and side slopes of 1.5:1. The homogenous embankment was constructed using a low plasticity clay (locally sourced Yolo loam) prepared to a relative compaction of 96%, based on the standard Proctor test, and a water content of 17.2% (dry of optimum). A vertical offset in the foundation was incrementally induced using a hydraulically actuated table with a maximum offset equal to 10% of the levee/dam height. Cameras and digital image tracking algorithms were used to measure deformation through 3D tracking markers embedded on the downslope surface. At low offset displacements, a rigid block rotation mechanism caused tensile cracks in the upthrown side which first initiated at the crest and was followed by a complimentary crack originating at the base of the embankment. At higher offset displacements, a third shear-induced crack was observed adjacent to the downthrown side. Following testing the model was dissected and the geometry of the transverse and shear cracks were mapped. Comparison of the results against the simplified geometries routinely used in engineering practice methods reveal notable differences.

KEYWORDS: Transverse cracking, concentrated leak erosion, embankment, crack propagation mechanisms, centrifuge testing.

1 INTRODUCTION

Cracking is one of the most critical hazards for earthen water-retaining structures, as it can lead to internal erosion through cracks in the embankment. Transverse cracks provide preferential pathways for water infiltration. Infiltrating water can initiate concentrated leak erosion (CLE) when the hydraulic shear stress along the cracks is sufficient to inhibit self-healing of the core due to soil swelling. If the initiation of CLE evolves into the continuation and propagation stages, breach failure becomes a likely consequence (Bonelli et al. 2013).

Transverse cracking in embankments may result from various causes, including differential settlement, seismic activity, desiccation, and anthropogenic actions. Among these causes, differential settlement is the primary factor contributing to crack development in embankments (He et al., 2022). Mechanisms of differential settlement related to transverse cracking include cross-valley settlement, settlement of compressible foundation soils, and differential settlement adjacent to spillways or abutment walls. Each of these mechanisms induces localized strains at structural interfaces such as abutment walls, spillways, or the embankment crest where cracking typically develops (Fell et al., 2008).

The USACE RMC (2025) toolbox, which incorporates the methodology, numerical simulations, and case histories presented by Fell et al. (2024), enables the estimation of crack dimensions, including width and depth, due to various causes. However, the case history data used to develop the toolbox are limited to settlement-to-embankment height ratios of up to 2% (Bolton et al., 2006; Fell et al., 2024). This limitation poses challenges when estimating crack dimensions for mechanisms involving larger settlement ratios, such as fault-induced offsets.

The geometry of transverse cracks plays a critical role in estimating the applied hydraulic shear stress responsible for initiating soil erosion within the crack. According to the RMC toolbox and previous literature, the crack geometry is typically assumed to be either a vertical tapered crack or a vertical parallel-sided crack under differential settlement scenarios (Fell et al., 2014; Savage et al., 2019). In both cases, the base of the crack is simplified as a straight horizontal line connecting the upstream and downstream of the embankment. Given that the applied hydraulic shear stress is a function of the crack's width and depth, as well as the average hydraulic gradient, inaccurate geometric assumptions may lead to erroneous evaluations of CLE potential.

Despite the critical influence of crack geometry on CLE evaluation, the conditions of potential cracks are conventionally determined using case history-based methodologies. While such methodologies facilitate practical assessments, there is a lack of supporting experimental data for understanding the formation and characterization of cracks. Inasmuch as accurate risk assessment of CLE depends on realistic representations of crack geometry, there is a need to establish a more rigorous, mechanics-based understanding of crack propagation mechanisms and crack formation in embankment deformation.

This study aims to provide experimental evidence to improve the mechanics-based understanding of crack initiation and propagation under foundation vertical offset, thereby contributing to the advancement of CLE risk assessment methodologies. A centrifuge model of a homogeneous embankment was constructed by compacting a low plasticity

clay inside a rigid rectangular container. A hydraulic actuator table incrementally imposed foundation vertical offsets of up to 10% of the embankment height. Four high-speed cameras were used to track the movement of markers placed on the downstream surface by recording their coordinates during testing. The test results presented herein focused on the sequence of crack propagation mechanisms and the evolving geometry of the primary transverse crack at crest.

2 EXPERIMENTAL TEST PROGRAM

The centrifuge test program simulates field-scale soil responses by replicating the in-situ stress profile in the model. The test, named as KWK01, was conducted at 40g using the 9 m radius centrifuge at the Center for Geotechnical Modeling at UC Davis, and will be archived on DesignSafe. All results and model descriptions are presented in prototype scale by applying relevant scaling laws (Garnier et al., 2007).

2.1 *Embankment model*

Yolo loam, a locally obtained clay soil with a liquid limit of 46 and a plasticity index of 21, was used to construct the embankment model, which had a height of 10 m and side slopes of 1.5:1 as shown in Figure 1(a). The soil was compacted in a flexible shear beam (FSB) container to 96% relative compaction of the standard Proctor test. The water content was 17.2%, which is dry of optimum, to induce brittle behavior of the soil (i.e., optimum water content is 18.7%).

The embankment model was built on a two-part base consisting of a static base and the hydraulically actuated table. The actuated table, supported on four pairs of actuators, was capable of inducing a maximum vertical settlement of 1 m (i.e., 10% of the embankment height). It was positioned beneath 1/3 of the embankment width [Figure 1(b)]. Additional details on the table construction are provided by Afolayan et al. (2024). To reduce side friction between the embankment and the FSB container during table settlement, Teflon sheets matching the shape of the embankment were attached to the inner sidewalls of the container and grease was applied to both the inside walls of the container.

2.2 *Instrumentation*

The model was instrumented with surface target markers, high-speed cameras, and linear potentiometers (LPs), with their locations indicated in Figure 1(b). To perform 3D stereophotogrammetry, seven quadrant markers were placed on the crest, and 26 markers were embedded on the downstream surface, spaced about 2 m in the vertical (z) direction and 4 m in the horizontal (x) direction. To avoid influencing crack initiation and propagation mechanisms, no markers were placed near the potential crack locations predicted by numerical simulations, which were conducted prior to the centrifuge test.

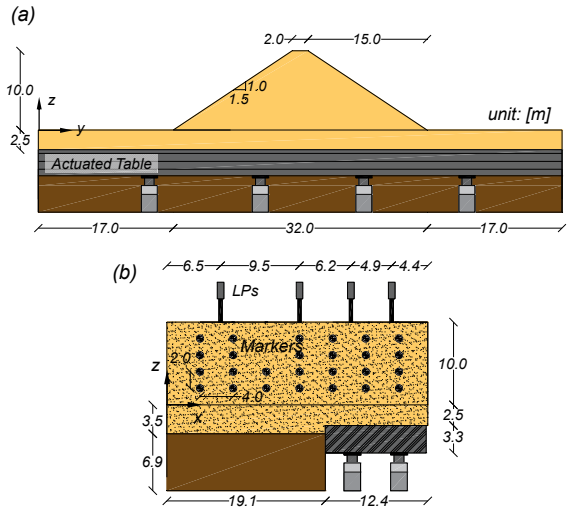

Figure 1. Centrifuge model: (a) cross-sectional view and (b) front view. All dimensions are in prototype scale.

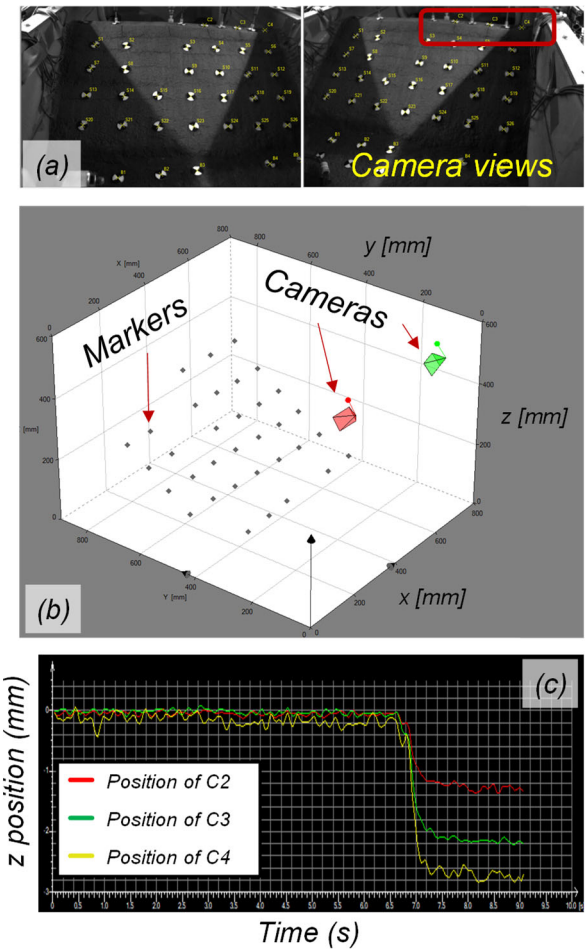

Figure 2. TEMA Classic 3D system: (a) two camera views of the model (red square indicates the positions of markers C2, C3, and C4); (b) coordinate system generated from markers; and (c) representative settlement time histories of markers recorded during the test.

Four Photron high-speed cameras were mounted on the FSB container to track and digitize the coordinates of the markers during testing. Marker coordinate changes were processed using TEMA Classic 3D, an advanced image- and motion-analysis software, as shown in Figure 2. Detailed information on the system can be found in Sinha et al. (2021).

Four LPs were installed along the crest to measure crest deformation and to validate vertical settlements obtained from the markers using the TEMA software. Six additional LPs were installed beneath the actuator table to measure the imposed settlement of the table during the test.

2.3 *Testing sequence*

The test program followed these steps. The embankment model was mounted on the centrifuge arm and spun up to 40g. Once the target g-level was reached, the solenoid valves connected to the hydraulic cylinders were opened to lower the actuator table. To capture the crack propagation mechanisms at each level of settlement, the total settlement was divided into eight incremental stages. Each stage imposed approximately 0.11–0.12 m of settlement on the model, which led to a total of 0.95 m of settlement at the final stage.

3 TEST RESULTS

3.1 *Overview – sequence of cracking*

The vertical offset induced the formation of three distinct cracks in the embankment model. These cracks developed in the following sequence: the primary transverse crack at the crest, a secondary transverse crack, and shear bands. The two transverse cracks formed on the upthrown side, while the shear band developed on the downthrown side. The development and sequence of these cracks are discussed in the following section using displacement vectors obtained from markers.

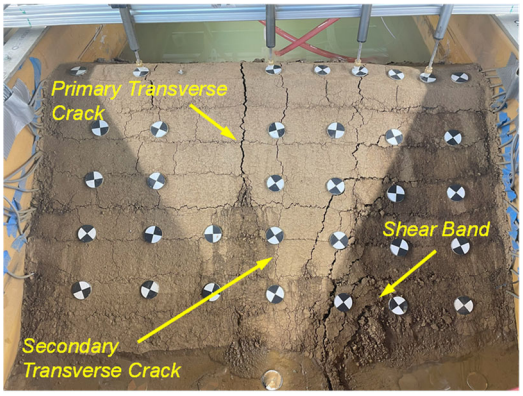

Figure 3. Developed cracks in the model after testing.

3.2 *Markers' displacement vector on downstream surface*

The displacement vectors of 26 markers on the downstream surface elucidate the initiation and propagation mechanisms of cracking in the embankment model (Figure 4). The vectors illustrate incremental displacements in the x–z plane at three settlement stages: (1) s/H = 0–2.3%; (2) s/H = 2.3–4.5%; and (3) s/H = 4.5–6.8%.

At the early stage of settlement (s/H = 0–2.3%), 12 markers on the downthrown side moved downward, while markers near the offset boundary exhibited both horizontal and vertical displacement components. Notably, marker S3, located on the upthrown side near the crest and offset boundary and labeled on Figure 4, moved toward the downthrown side in both horizontal and vertical directions, whereas markers at x = 8–12 m with z = 2–8 m on the upthrown side remained stationary. This indicates a horizontal gap developed between markers S2 and S3, which led to the initiation of the primary transverse crack. Simultaneously, markers at x = 16 m with z = 2–4 m on the upthrown side did not move while markers on the upthrown side were displaced. This relative displacement near the toe and offset boundary initiated the secondary transverse crack.

A rotational mechanism explains the early-stage response of the embankment (Figure 5). As the vertical offset induces tensile and shear strains within the embankment, three distinct regions emerge to accommodate the imposed settlement: (1) an upthrown side, (2) a rotational zone, and (3) a downthrown side. The downthrown side moves downward with the actuator table. The upthrown side remains stationary. Between these sides, the rotational zone rotates to accommodate the induced strains. A primary transverse crack forms at the interface between the upthrown side and the rotational zone when the induced strain exceeds the tensile failure strain of the soil. The observed response is consistent with findings from previous studies (Bray et al., 1993; Ng et al., 2012).

At the stage when s/H = 2.3–4.5%, the markers on the upthrown side remained stationary whereas marker S4 experienced horizontal displacement. This relative movement created a horizontal gap between markers S3 and S4, enabling the secondary transverse crack to propagate upward from the

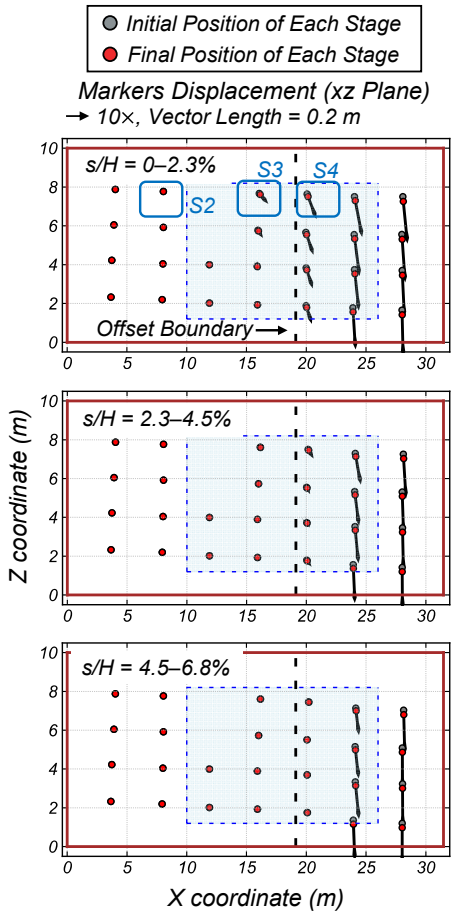

Figure 4. Displacement vectors of downstream markers in the x–z plane at each settlement stage.

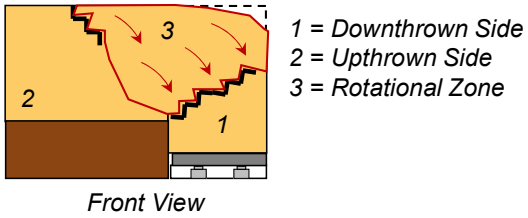

Figure 5. Schematic illustration of the rotational mechanism in the embankment.

toe toward the crest. Given that the upthrown side markers showed no additional movement beyond s/H = 2.3%, the primary transverse crack did not widen or deepen further after this stage. Although the relationship between crack development and the imposed s/H is governed by the tensile failure strain of the soil, the s/H of 2% appears sufficient to fully develop the primary transverse crack at the crest under the tested conditions.

At the stage when s/H = 4.5–6.6%, the markers at x = 16–20 m with z = 2–8 m near the offset boundary, including those embedded on the downthrown side, remained stationary while 8 other markers at x = 24–28 m with z = 2–8 m on the downthrown side moved downward with the actuator table as a rigid body. This relative displacement developed shear bands above the downthrown side.

3.3 *Crack geometry*

After the test, the location of the base of the primary transverse crack in the embankment was manually identified during the dissection of the model (Figure 6). Contrary to the assumptions in the RMC toolbox and previous literature, the crack geometry was found to a bell-curved shape (concave-downward arc)

rather than a straight bottom line. The secondary transverse crack exhibited a similar geometry upon dissection, consistent with the findings of Afolayan et al. (2024).

The actuator-induced differential settlement imposes specific levels of shear and tensile strain in the model, regardless of the soil strength, indicating that the testing condition is strain-controlled. Tensile cracking initiates when the minor principal stress of the soil reaches its tensile strength. As a result, cracks are more likely to develop near the embankment surface, and the final crack path tends to follow the embankment geometry, which in turn is governed by the distribution of the minor principal stress.

For CLE evaluation, the bell-shaped crack geometry would require a different approach for estimating the hydraulic gradient within the crack. This geometric consideration would have a direct impact on the estimation of the applied hydraulic shear stress.

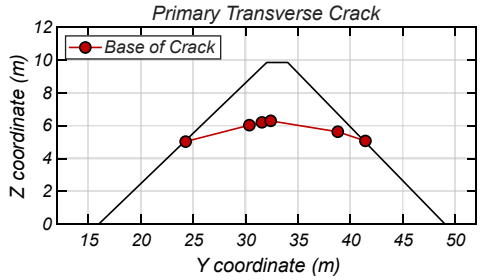

Figure 6. Cross-sectional view of the base of the primary transverse crack in the model.

4 CONCLUSIONS

This paper investigated crack initiation and propagation mechanisms in a centrifuge model of a 10 m-high (prototype) homogeneous embankment. A centrifuge model of the embankment was constructed and subjected to a vertical offset in the foundation.

The three distinct cracks and shear bands were identified as the offset was induced: the primary transverse crack at the crest, the secondary transverse crack propagating from the toe upwards to crest, and the shear bands arcing over the downthrown side. Tracking of displacement markers on the face of the embankment showed a rotational mechanism, which elucidated the development of these cracks and shear bands. During the vertical offset, the embankment model exhibited three distinct regions: a rigid body movement of the downthrown side; no movement of the upthrown side, and a rotational zone between the other two. The primary transverse crack formed between the shear zone and the upthrown side and was fully developed at the settlement ratio of 2%.

The transverse cracks exhibited the bell-curved geometry, deviating from the straight bottom line typically assumed in the existing methods to analyze CLE potential through cracks. The variation in crack depth and width across the embankment directly affects the hydraulic gradients and associated hydraulic shear stresses inside the cracks for a given reservoir level. Further work is on-going to understand how this change in geometry affects the likelihood of CLE progressing to a breach.

These experimental findings discussed the initiation and sequential development of cracking. Moreover, the test results illustrate the complexity of cracking processes and the uncertainties inherent to predicting crack depths, widths, shapes, and locations. Centrifuge modeling for a broader range of embankment and loading conditions could provide the data and insights necessary for developing a mechanics-based procedure for evaluating cracking and CLE potential in embankment dams and levees.

5 ACKNOWLEDGEMENTS

The authors would like to thank the staff at the UC Davis Center for Geotechnical Modeling for their dedicated support and technical assistance throughout the centrifuge testing program. This material is based upon work funded by the National Science Foundation (Natural Hazards Engineering Research Infrastructure (NHERI) facility at the University of California at Davis (CMMI-1520581) and grant (CMMI 2047402) and the California Department of Water Resources (Agreement 4600014658). Any opinions, findings, and conclusions or recommendations are those of the author(s) and do not necessarily reflect the views of the National Science Foundation.

6 REFERENCES

Afolayan, O., Montgomery, J., Wilson, D., Boulanger, R., Babchanik, A., Maggio, M. and Bille, Y., 2024. *ODA01: Centrifuge modelling of vertical differential settlement-induced cracks in a levee*. [dataset] DesignSafe-CI. Available at: https://doi.org/10.17603/ds2-ftkc-v575 [Accessed 6 Aug. 2025].

Bolton, A., Brandon, T.L., Duncan, J.M., Mitchell, J.K. and Tiwari, B., 2006. *Literature review: Depth of cracking in dams worldwide*. Blacksburg, VA.

Bonelli, S., Fell, R. and Benahmed, N., 2013. Concentrated leak erosion. In: Bonelli, S., ed., *Erosion in geomechanics applied to dams and levees*. Chichester: Wiley, 271–341.

Bray, J., Seed, R. and Seed, H., 1993. 1g small-scale modelling of saturated cohesive soils. *Geotechnical Testing Journal*, 16(1), 46–53.

Fell, R., Foster, M., Cyganiewicz, J., Sills, G., Vroman, N. and Davidson, R., 2008. *A unified method for estimating probabilities of failure of embankment dams by internal erosion and piping*. Sydney, Australia.

Fell, R., Foster, M., Cyganiewicz, J., Davidson, R. and Sills, G., 2024. *Methods for estimating probability of failure of embankment dams by internal erosion and piping (The Piping Toolbox 2024)*. Sydney, Australia.

Fell, R., MacGregor, P., Stapledon, D., Bell, G. and Foster, M., 2014. *Geotechnical engineering of dams*. [online] 2nd ed. Boca Raton, FL: CRC Press. Available at: https://www.routledge.com [Accessed 6 Aug. 2025].

Garnier, J., Gaudin, C., Springman, S.M., Culligan, P.J., Goodings, D., Konig, D., Kutter, B., Phillips, R., Randolph, M.F. and Thorel, L., 2007. Catalogue of scaling laws and similitude questions in geotechnical centrifuge modelling. *International Journal of Physical Modelling in Geotechnics*, 7(3), 1–23.

He, K., Fell, R. and Song, C., 2022. Transverse cracking in embankment dams resulting from cross-valley differential settlements. *European Journal of Environmental and Civil Engineering*, 26(3), 995–1021. [online] Available at: https://www.tandfonline.com [Accessed 6 Aug. 2025].

Ng, C.W.W., Cai, Q.P. and Hu, P., 2012. Centrifuge and numerical modeling of normal fault-rupture propagation in clay with and without a preexisting fracture. *Journal of Geotechnical and Geoenvironmental Engineering*, 138(12), 1492–1502.

Savage, S., Douglas, K., Fell, R., Peirson, W. and Berndt, R., 2019. Modeling the erosion and swelling of the sides of transverse cracks in embankment dams. *Journal of Geotechnical and Geoenvironmental Engineering*, 145(5).

Sinha, S.K., Kutter, B.L., Wilson, D.W., Carey, T.J. and Ziotopoulou, K., 2021. *Use of Photron cameras and TEMA software to measure 3D displacements in centrifuge tests*. UCD/CGM21/01. Davis, CA: Center for Geotechnical Modeling, UC Davis.

U.S. Army Corps of Engineers Risk Management Center (USACE RMC), 2025. *RMC Concentrated Leak Erosion (Cracking) Toolbox* [software] Version 2.1. Institute for Water Resources. Available at: https://www.rmc.usace.army.mil/Software/RMC-Toolboxes/Internal-Erosion-Suite/ [Accessed 22 Jul. 2025].